



# Atmospheric plasma spraying of nanocrystalline SiC particle reinforced MoSi<sub>2</sub> prepared by mechanically activated annealing process

Mostafa Salek<sup>1</sup> · Saeed Reza Bakhshi<sup>1</sup> · Mohammad Erfanmanesh<sup>1</sup>

Received: 12 April 2017 / Revised: 13 April 2017 / Accepted: 12 January 2018 / Published online: 4 February 2019  
© Australian Ceramic Society 2019

## Abstract

The mechanically activated annealing process was adopted to synthesize nanostructure MoSi<sub>2</sub>–SiC powders containing different SiC contents using Mo, Si, and SiC powders. Atmospheric plasma spraying technique was used to deposit the agglomerated powders of MoSi<sub>2</sub>–SiC nanocomposite under inert conditions on a nickel substrate. Phase identification and microstructural characteristics of the nanopowders and coatings were evaluated by X-ray diffraction (XRD), scanning electron microscopy (SEM), and qualitative energy-dispersive spectroscopy (EDS). The microstructure of the plasma-sprayed coating consists of  $\alpha$  and  $\beta$ -MoSi<sub>2</sub>, SiC, Mo<sub>5</sub>Si<sub>3</sub>, and a trace of SiO<sub>2</sub> phases. It can be concluded that mechanically activated annealing synthesis with agglomeration is an effective method for the preparation of high-melting-point refractory compounds for using in plasma spraying process. The measured adhesion strength, microhardness, and roughness results of MoSi<sub>2</sub>–SiC coatings are also reported in the present work.

**Keywords** MoSi<sub>2</sub>–SiC · Nanostructure · Atmospheric plasma spraying · Mechanically activated annealing

## Introduction

With the development of research on nanomaterials, a great attention has been dedicated to the preparation and characterization of nanostructured coatings. Many methods can be implemented to fabricate nanostructured coatings. Recently, the preparation of nanostructured coatings by thermal spraying has become an active field of interest. Because of grain size effects and interface effects, nanostructured coatings have many superior properties compared with those of conventional coarse-grained coatings, e.g., mechanical properties, wear resistance, and thermo-physical properties [1, 2]. Thermal spraying has been reported as a convenient method to prepare a nanostructured coating. One advantage of the thermal spraying of the nanostructured coating is that the aggregation of nanostructured powders has no disadvantageous effect on

the spray process of nanostructured coating which is harmful to the sintering of ceramics [2].

MoSi<sub>2</sub> might be potentially used as protective coatings for high-temperature applications because of its high melting point (2030 °C) and its high-temperature oxidation resistance [3]. One of its main applications is in oxidation-resistant coatings [4]. Moreover, MoSi<sub>2</sub> is a good wear-resistant material and well known for its applications at high-temperature corrosive and oxidative environments because of its high hardness and elastic modulus. MoSi<sub>2</sub> is also used as a wear-resistant coating for its applications in both room and high-temperature environments [5]. However, the main disadvantages, limiting its use, are its low fracture toughness at lower temperatures (< 1000 °C) and the low strength and creep resistance at high temperatures (> 1200 °C) [5]. Reinforcing MoSi<sub>2</sub> with SiC shows an improvement in its low toughness at room temperature and low creep resistance at temperatures above the brittle–ductile transition temperature of approximately 700–1000 °C [6, 7]. Preparing this composite in nanostructure is another method for improving its mechanical properties such as room temperature toughness [7].

Conventionally, silicides are processed by arc melting, silicidation of elemental powders, and reduction of metal oxide. These processes are energy-intensive and require long

✉ Saeed Reza Bakhshi  
bakhshsr@mut-es.ac.ir

<sup>1</sup> Department of Materials Engineering, Malek Ashtar University of Technology, Shahin Shahr, Isfahan, Iran

**Table 1** The chemical analysis of nickel substrate

Substrate	Chemical analysis (wt%)													
	Ti	Nb	Hf	Cr	Co	Al	S	P	Si	C	Mn	Mo	Ni	Fe
Nickel	< 0.1	< 0.1	< 0.3	< 5	< 5	0.131	–	–	–	–	< 0.03	< 0.3	89.31	–

homogenization times in order to obtain desired products. The loss of silicon by volatilizations during arc melting can result in the formation of undesirable intermediate phases. In addition, the silicide powders obtained by these routes have high oxygen contents and other impurities, which are not desired for high-temperature structural applications. It is possible to obtain high-purity powders by applying reactive processing techniques such as mechanical alloying (MA), combustion synthesis (CS), and displacement reactions. In a reactive process, constituent elements/compounds react in situ and produce desirable products [8].

MoSi<sub>2</sub> has been synthesized by various methods, such as casting, conventional arc melting, and powder metallurgy including sintering, hot pressing, and self-sustaining combustion (SHS). However, the high melting point and the line compound in the phase always limit the fabrication of MoSi<sub>2</sub> by these conventional methods [9]. Various methods including furnace technique [10], mechanical mixing [11], reaction bonding [12], and SHS [13] are applied to obtain MoSi<sub>2</sub>–SiC composites.

Gaining intermetallics by direct MA methods is a difficult task since it takes a substantial matter of time (sometimes hundreds of hours) to synthesize the end products. The long ball-milling time will also introduce a high level of contamination coming from the container and the milling media. In addition, it is difficult to obtain the pure compound by reactive sintering synthesis (RS) technique as sometimes this needs a high sintering temperature and the powders oxidize easily. Hence, it is very important to combine the advantages of mechanical alloying and reactive synthesis, as well as avoiding their shortcomings. The powders undergo short ball-milling time, without amorphous phase and narrow contamination. However, the time and temperature of synthesis reaction can be lowered [14].

**Table 2** The operating parameters of atmospheric plasma spray

Parameters	MS10 and MS20	MS30
Current (A)	750	650
Gas Ar (slpm)	30	47
Gas N <sub>2</sub> (slpm)	5	–
Gas H <sub>2</sub> (slpm)	–	10
Carrier gas Ar (slpm)	3	2.2
Spray distance (mm)	100	50

Mechanically activated annealing (M2A) is a process that combines short mechanical alloying duration with a low-temperature isothermal annealing. The combination of these two steps has been found to be effective in producing different refractory materials such as silicides [15]. This fabrication route offers the possibility of lower sintering temperatures than are usually needed since these elemental powders are softer than prealloyed powders. In addition, the internal heat generation as the elemental powders react during sintering leads to an additional short high-temperature excursion. Finer microstructures are possible by such processing methods, both because of the lower temperatures involved and the fine starting structures of the milled powders [12].

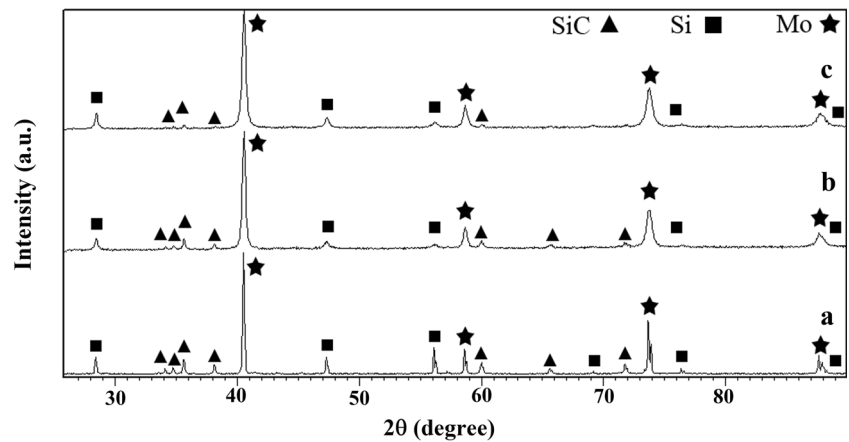
Such a solid-state processing method has been successfully applied to activate the phase transition induced by solid-state diffusion in the case of FeSi<sub>2</sub>, MoSi<sub>2</sub>, and WSi<sub>2</sub>. Besides, it has been found as an efficient method for the low-temperature synthesis of refractory nanomaterials. In the case of the Mo–Si system, the M2A process was found as a very suitable method to produce nanocrystalline MoSi<sub>2</sub> phase. Indeed, the first mechanical M2A step leads to activation of the three-dimensional element distribution which reacts 400 °C below the temperature of the classical processes, i.e., 800 °C instead of 1200 °C [16].

In this work, a new method is introduced for the manufacture of nanocrystalline MoSi<sub>2</sub>–SiC powders as a feedstock for thermal spraying by means of a milling process followed by a heat treatment and also their processing through atmospheric plasma spraying (APS). Based on X-ray diffraction (XRD) analysis and scanning electron microscope (SEM), the as-milled powders, M2A end products, and coatings were characterized. Moreover, microhardness, roughness, bonding strength, and thickness of coating were measured.

## Experimental procedures

Mo (purity > 96%, particle size < 12 μm), Si (purity > 95%, particle size < 10 μm), and SiC (purity > 98%, particle size < 7 μm) powders were used as starting materials and manually mixed for 15 min. The MA was performed using an Ar atmosphere-controlled attritor milling with a stainless steel vial and balls made of the roller bearing steel (10 mm in diameter) [17]. The mixed stoichiometric composition of Si and Mo (for MoSi<sub>2</sub>) and SiC powder (10, 20, and 30 vol%, denoted as MS10, MS20, and MS30, respectively) were placed in the vial

**Fig. 1** X-ray diffraction patterns of MS20 mixture **a** before, **b** after 20 h, and **c** after 19 + 1-h MA treatment



and rotated with a speed of 365 rpm for 20 h [15]. The weight of the ball to charge ratio was taken as 20:1. To reduce the excessive friction and increase mixing efficiency, 0.5 wt% of stearic acid was added as a process control agent (PCA). This acid also prevented any cold welding that could occur during the MA process [15]. Next, the annealing of the as-milled powders was carried out under argon inert gas atmosphere at 1100 °C for 7 h with a heating rate of 10 °C/min [18]. The annealed powders

were agglomerated with a mixture of deionized water and a water-soluble polymer as a binder (carboxymethyl cellulose). The well-stirred slurry was dried by hot air to form agglomerated chunks. The agglomerated powder was sifted to the grain size fraction from 45 to 125 μm, relevant for the thermal spraying. The apparent density and flow rate of agglomerated powders were measured according to ASTM B212-99 [19] and ASTM B213-03 [20], respectively.

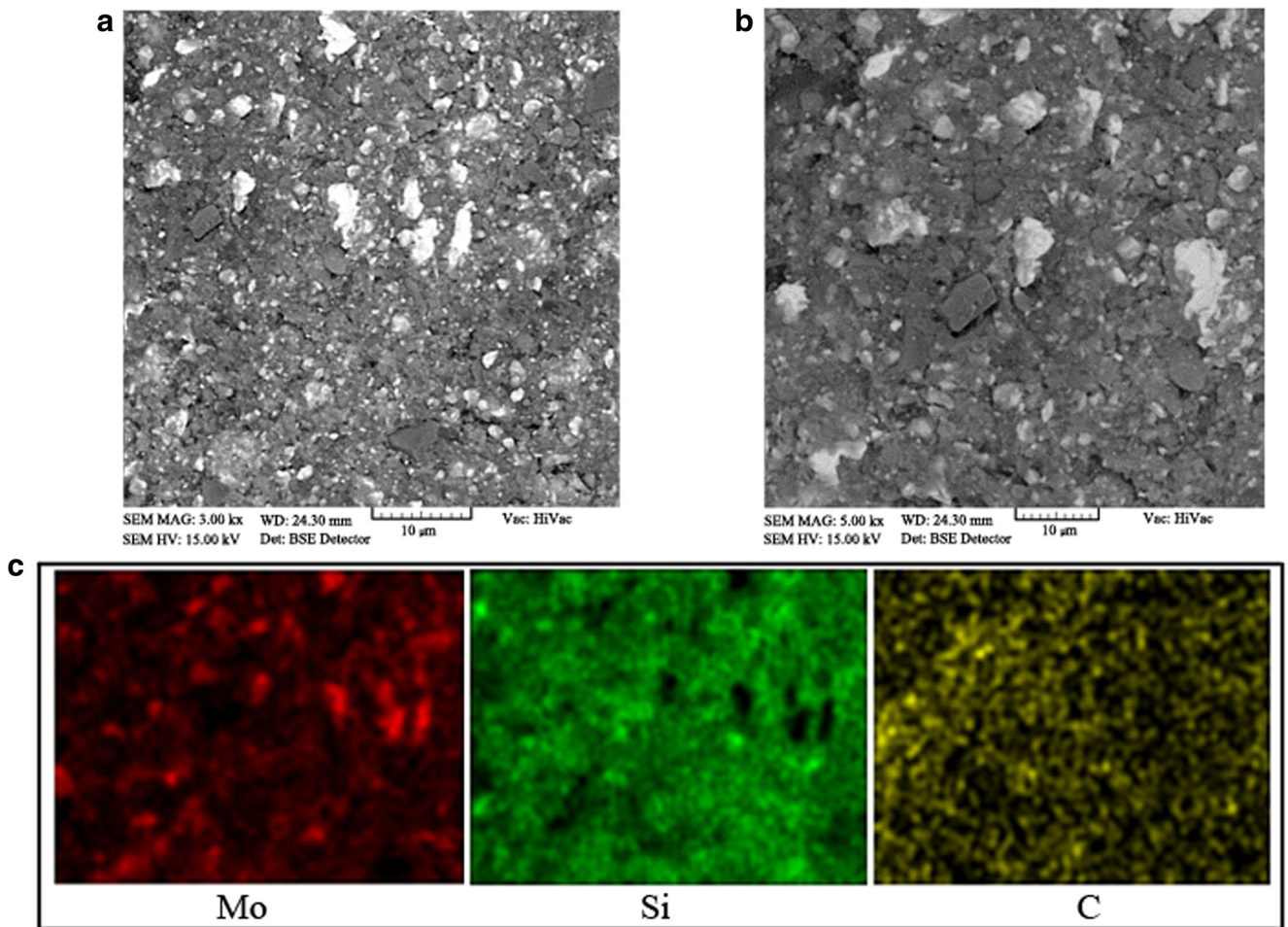
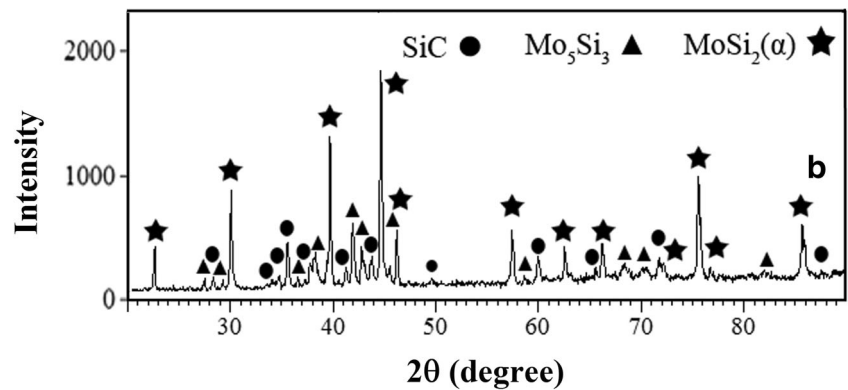


**Fig. 2** **a, b** Backscattered electron (BSE) images of mechanical alloying MS20 powders milled for 19 + 1 h at different magnifications; **c** map analyses of **a**

**Fig. 3** X-ray diffraction patterns of annealing samples of MS20 powders at 1100 °C for 7 h



Atmospheric plasma spraying technique (Metallization Plasma PS50M-PC, UK) equipped with a PS50MPF/B torch was used to deposit the agglomerated powders of MoSi<sub>2</sub>–SiC composite under inert conditions onto a substrate. Nickel (with the chemical analysis listed in Table 1) was selected as a substrate in this work. The substrate was grit-blasted by SiC particles of 20 meshes with 10-cm distance from the nozzle to sample for 20 s with 90° and then cleaned with ethanol prior to the spraying process. The average roughness (Ra) of the substrate was 4.51 ± 2 μm after grit blasting. To prevent oxidation of powders during spray, a

spray torch with argon shielding gas (ASPS) was used [21]. The optimized spray operating parameters are summarized in Table 2.

The microstructure and particle morphology of the products were investigated using scanning electron microscope (VEGA-XMU, TESCAN) equipped with energy-dispersive spectroscopy (EDS). In addition, the phase analysis of the samples was studied using a Philips powder X-ray diffractometer with Ni-filtered Cu Kα radiation operating at 40 kV and 30 mA. A scan with a step size of 0.05° and counting time of 1 s was applied at each step. The crystallite sizes of powders

**Table 3** Average crystallite size of samples by the WH equation

Samples	Crystallite size (nm)				
	Mo	Si	SiC	MoSi <sub>2</sub>	Mo <sub>5</sub> Si <sub>3</sub>
Mo + Si + SiC before MA	8530	7780	4500	–	–
20-h MA	28	32	30	–	–
19 + 1-h MA	39	45	200	–	–
20-h MA and heat treatment at 1100 °C for 7 h	–	–	290	78	59

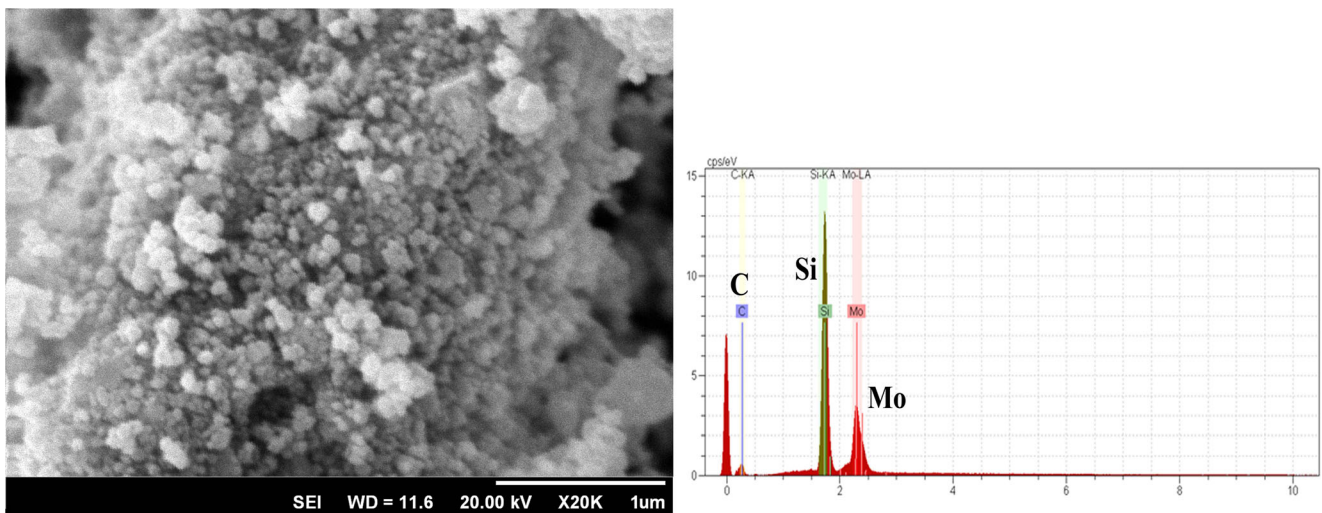


**Fig. 4** SEM image of the sample MS20 milled for 19 + 1 h and heated at 1100 °C for 7 h

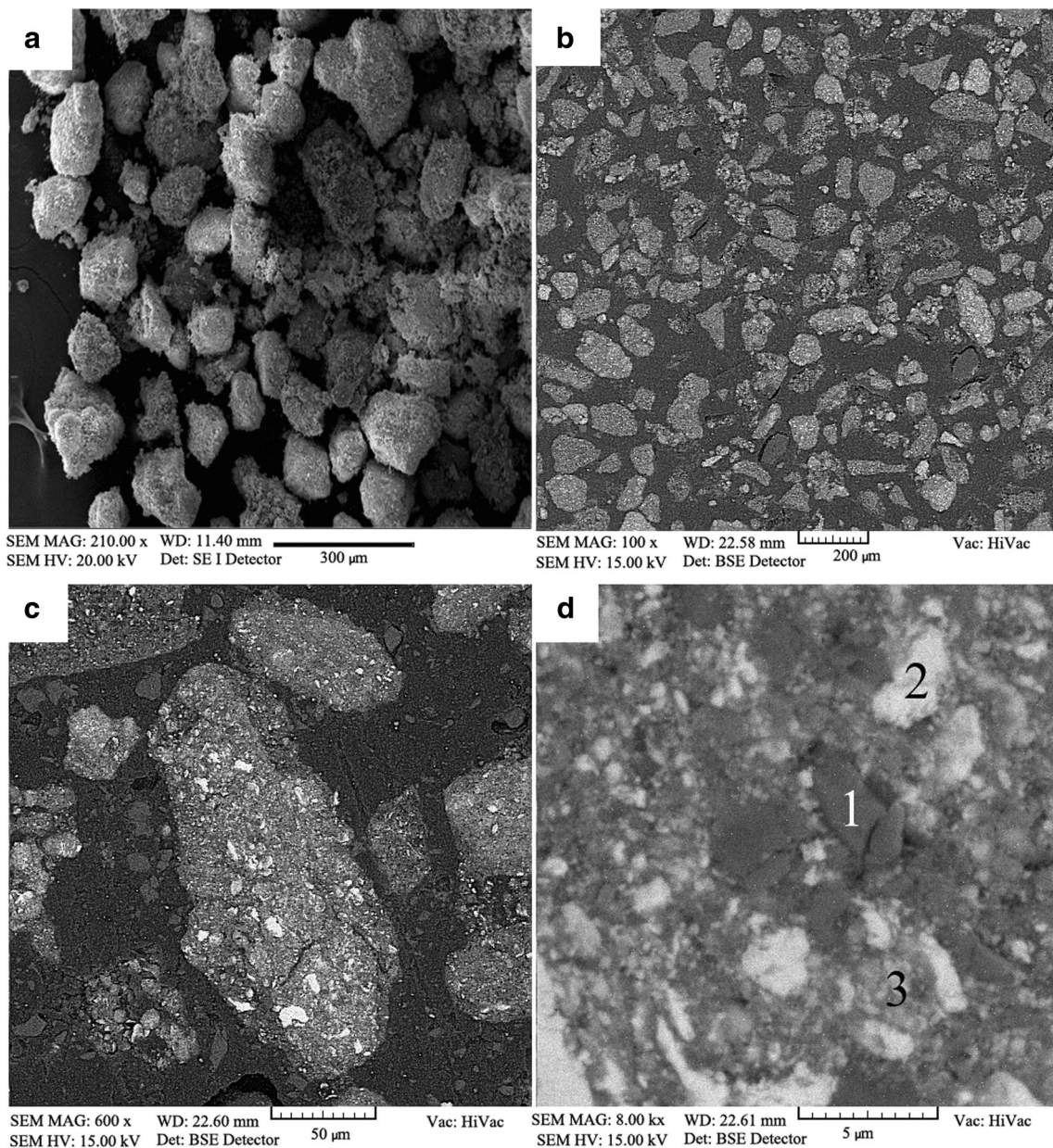


**Fig. 5** SEM images of annealed MS20 powders after agglomeration: **a** SE and **b–d** BSE mode at different magnifications

were obtained from XRD analyzing data using Williamson–Hall (WH) Eq. 1 [22, 23]:

$$\Delta(2\theta)\cos\theta = \frac{0.9\lambda}{d} + 4\varepsilon\sin\theta \tag{1}$$

where  $\Delta(2\theta)$  is the full width at half maximum (FWHM) of the Bragg peaks (in radians),  $\theta$  is the Bragg angle of the analyzed peak,  $\lambda$  is the wavelength of the X-rays used in nanometers (0.154056 nm for Cu  $K\alpha$ ),  $d$  is the average crystallite size, and  $\varepsilon$  is the average internal strain. The average internal strain can be estimated from the linear slope of  $\Delta(2\theta)\cos\theta$  versus  $\sin\theta$ , and the average crystallite size can be estimated from the intersect of this line at  $\sin\theta = 0$ .

Through the microhardness test, a Zwick type (3212, Germany) device with a diamond of Vickers geometry was utilized. The load of 0.5 N was applied 15 s on the sample and the Vickers microhardness determined as HV0.05. The roughness of coatings was measured after spray operation using the fully automatic Mitutoyo machine. Adhesion strength of coatings was measured according to ASTM C0633 [24], using a universal Zwick puller device with the speed of 1 mm/min and adhesive resin from Scotch-Weld Company (SW2214 code). The cylindrical samples were used for plain carbon steel with a diameter of 2.5 cm, the height of 3.5 cm, and coating thickness of  $400 \pm 20 \mu\text{m}$ . To determine microhardness, roughness, and adhesion strength of the samples, the tests were repeated on five samples and their average was presented.

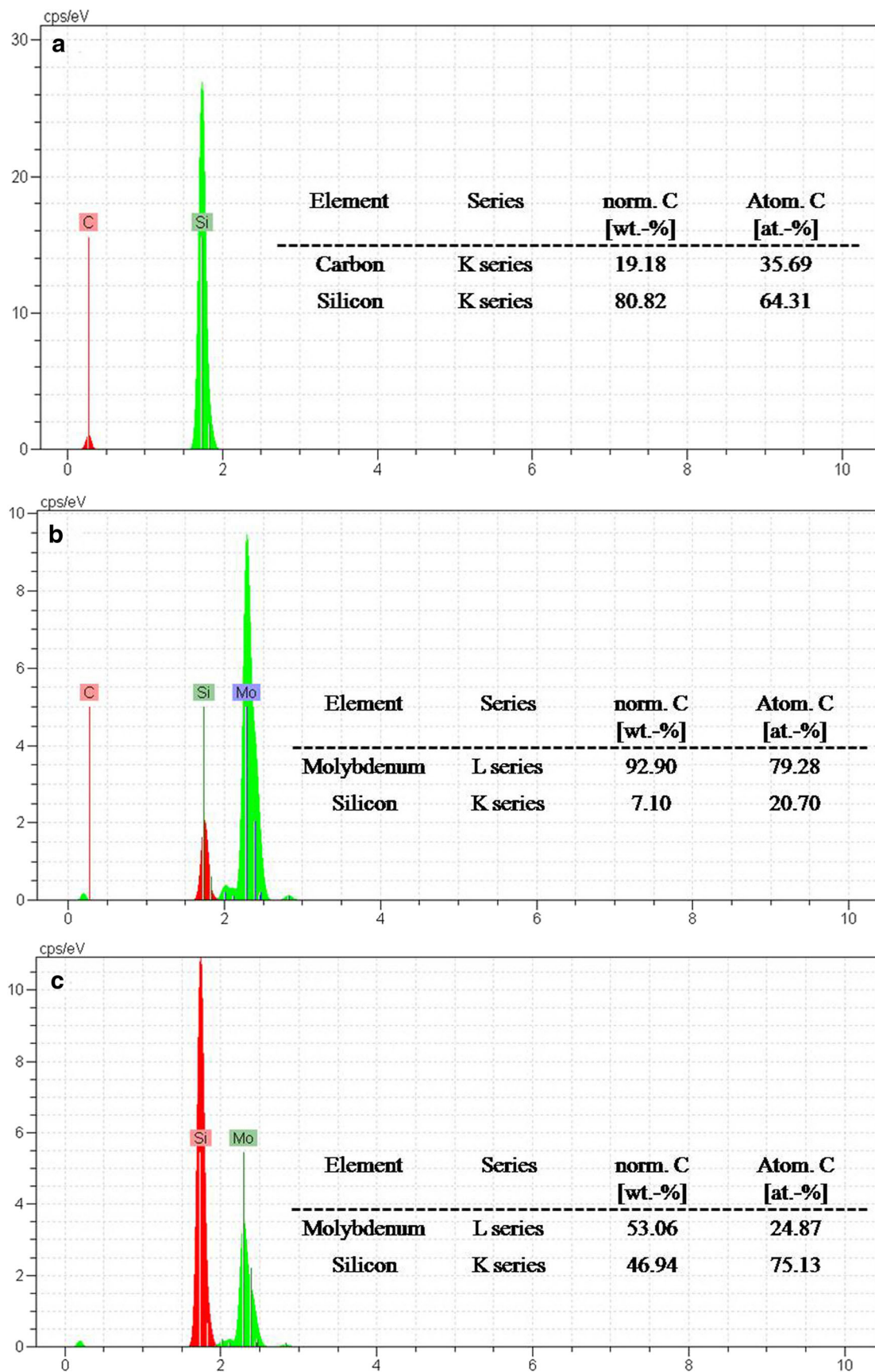
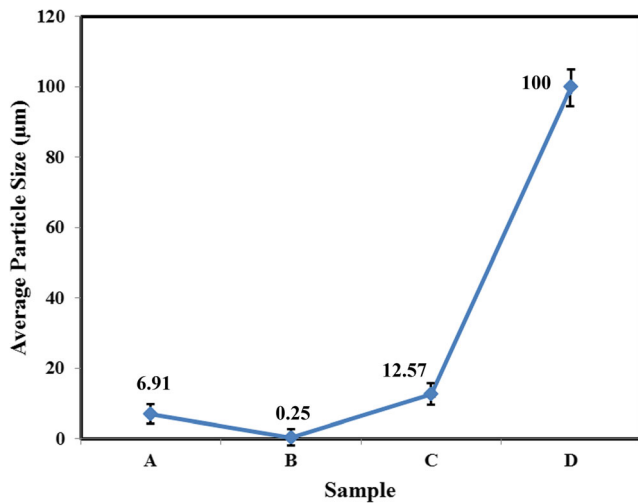


Fig. 6 EDS analyses of the points a 1, b 2, and c 3 on Fig. 5d



**Fig. 7** The variation of average particle size **a** before MA, **b** after MA, **c** after heat treatment, and **d** after agglomeration

## Results and discussion

### Characterization of the MoSi<sub>2</sub>-SiC powders

Due to the high hardness of SiC and to prevent powder contamination, first Mo and Si powders were milled for 19 h and then SiC powder was added to Mo + Si mixture and milled for 1 h. The results of XRD patterns compared to Mo + Si + SiC mixture mechanical alloyed for 20 h are shown in Fig. 1. Comparing the XRD patterns of activated powders with non-activated powder in this figure reveals a modification of the peak intensity and shape in the case of as-milled powders. This behavior is due to the decrease in crystallite size and the increase in residual lattice distortion during the mechanical

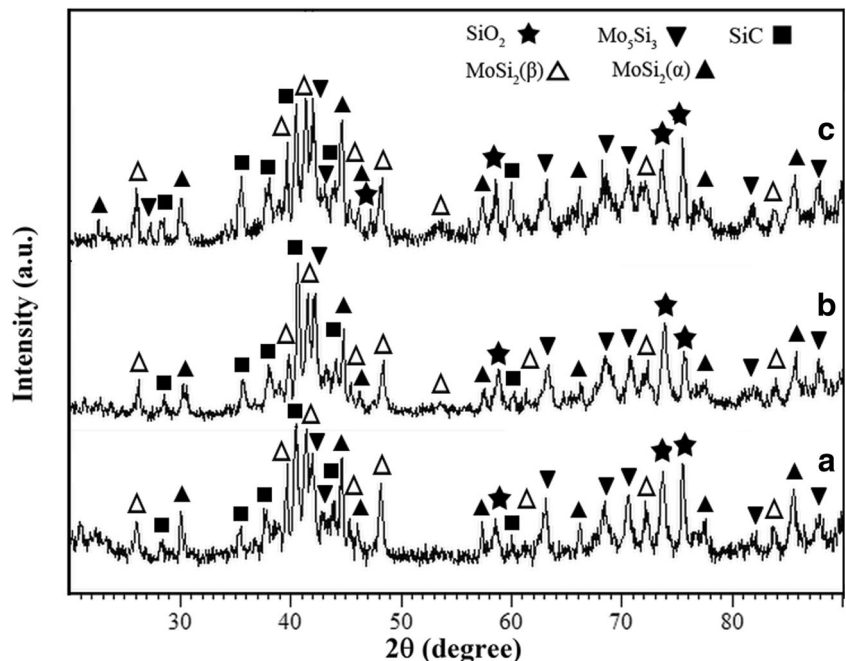
activation process. Due to mechanical stresses in the mechanical alloying process, crystal defects such as dislocations and point defects were increased [25]. The formed defects increase lattice strain and energy, so it makes unstable. The dislocations rearrange themselves to a lower energy state leading to the formation of sub-grain. At longer process of mechanical alloying and therefore higher plastic deformation and generation of more dislocations, the misorientations between sub-grains at their boundaries increase and finally they convert to high angle boundaries and become smaller crystallites [26].

The results of the sample milled for 19 + 1 h are similar to those for the sample milled for 20 h. Thus, to produce the powder, SiC powder was milled with a mixture of Mo and Si powders for 1 h. It should also be noted that sharp peaks in Fig. 1 are for the powders mixture before MA treatment. After milling process, the intensity of both Si and SiC reflection peaks decreased. In addition, the broadening of peaks is related to the fine structure, which is formed during milling of powders. Another explanation for such a broadening might be the introduction of internal strains [27].

As can be seen in Fig. 1, the spectra indicate no chemical reaction between Mo, Si, and SiC during the ball-milling process. Lack of any shift in the peak positions of Mo in MA-ed spectra leads to the conclusion that no reciprocal solid solution has occurred.

The SEM micrographs of the milled powders are shown in Fig. 2a, b. It can be seen from the morphologies that the particle size is uneven. Moreover, the light irregular particles were detected as Mo by the EDS analysis. Figure 2c shows map analyses of Fig. 2a that represents the uniform distribution of Mo, Si, and SiC atoms in the milled powder.

**Fig. 8** XRD patterns of as-sprayed **a** MS10, **b** MS20, and **c** MS30 coatings



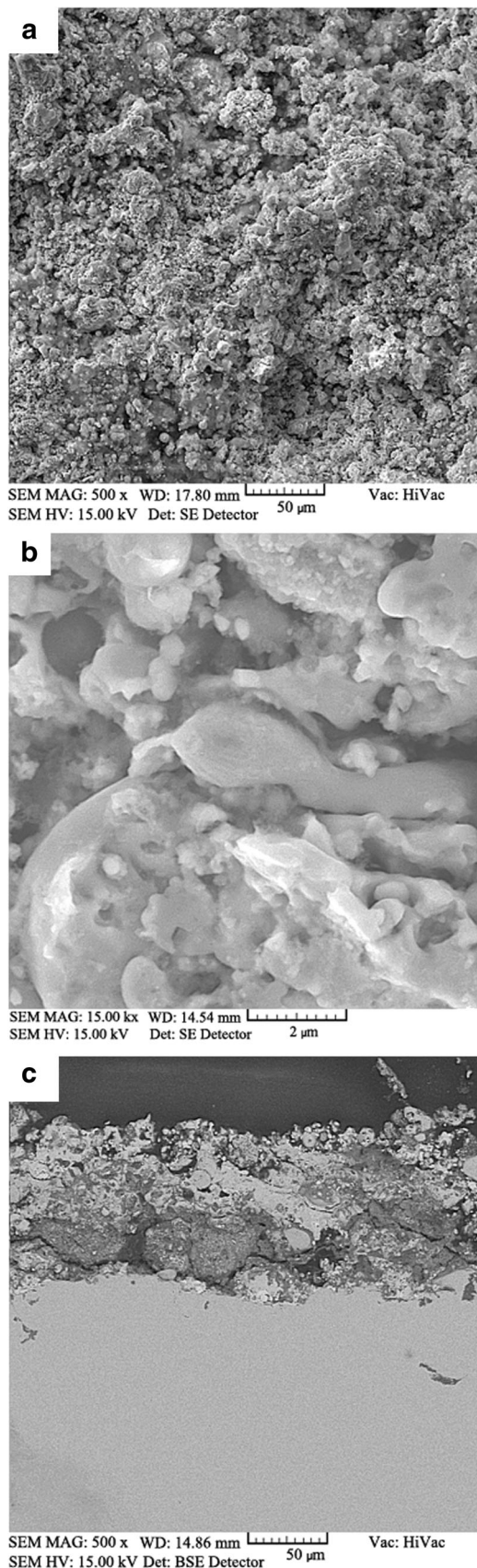


**Fig. 9** SEM picture of the MS20 coating: **a** on the surface, **b** fracture surface, and **c** polished cross section

In summary, on the basis of SEM and XRD studies, the structure of as-milled powders may be considered particles composed of molybdenum, silicon, and silicon carbide without Mo–Si intermetallic compound formation.

The XRD patterns of the powder mixture milled for 19 + 1 h and annealed in Ar atmosphere at 1100 °C for 7 h are shown in Fig. 3. The annealing leads to the almost complete reaction since the main phase detected is MoSi<sub>2</sub> and the Mo and Si peaks disappear completely. This behavior is similar to the result of the reactive synthesis of MoSi<sub>2</sub> + 30 wt% SiC stoichiometry compact at 1450 °C at a heating rate of 5 °C/min [28]. Thus, the effect of ball milling on the reduction of the reactive temperature in the present work is considerable.

Undergoing annealing at 1100 °C for 7 h might lead to the formation of MoSi<sub>2</sub> and SiC peaks, as well as a small amount of Mo<sub>5</sub>Si<sub>3</sub>. The results of mechanical alloying and heat treatment of powder mixture indicate that MoSi<sub>2</sub>–SiC composite can be obtained by the ball milling of the powders and heat treatment. Because of MA process and its energy content, Mo atoms are absorbed on the Si particle surface (or vice versa) and form primary bonds. Molybdenum and silicon powders with the higher surface energies can react together and form MoSi<sub>2</sub> [29]. In this way, the energy of the powders can be improved by mechanical alloying because the energy of the system may exceed the barrier energy of the formation of MoSi<sub>2</sub> as a result of the exterior energy of the heat treatment. The heat treatment causes the Mo and Si to react together. Other effects of heat treatment are the stress relieving and grain growth, which lead to reducing in the strain and peak widths [14].

It can be seen that the glassy SiO<sub>2</sub> phase characteristic of conventional powder-processed MoSi<sub>2</sub> is effectively eliminated by combining mechanical alloying and annealing. This method, which can be termed mechanically activated annealing (M2A), is useful for the preparation of refractory materials. The results of the XRD patterns (Fig. 1a) reveal that no phase reactions take place during the milling process, whereas the heat treatment makes the powder to react as expected (Fig. 3). Without the heat treatment and the pre-reaction of the powder in the course of this, unbound silicon and molybdenum would oxidize if they came into contact with air-oxygen and would prevent further phase formation during the thermal spraying [3]. The average of crystalline sizes was measured after 20 h of milling and after heat treatment and reported in Table 3. Evidently, the milling and heat treatment processes decreased and increased the crystallite size, respectively.

It should be noted that XRD intensities not only depend on the phase content but also change with many other factors such as the crystallite size, lattice strain, and degree of crystallinity [15, 22].

Figure 4 presents the SEM images of powders after MA and heat treatment. As shown in the SEM micrograph, it may be concluded that the particle size is reduced from about 10 to

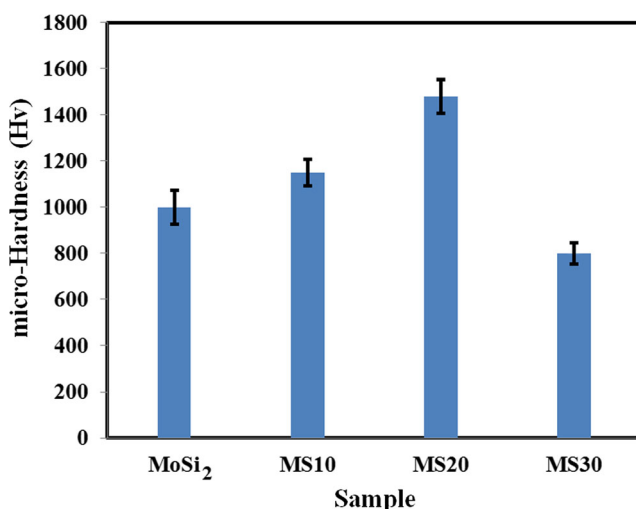


**Table 4** The results of roughness, microhardness, and adhesion strength for different coatings

Type of coating	Surface roughness (Ra) ( $\mu\text{m}$ )	Adhesion strength (MPa)	Microhardness (HV0.05)
MoSi <sub>2</sub> coating [18, 21]	4.46 $\pm$ 2	27 $\pm$ 3	1000 $\pm$ 50
MS10	5.62 $\pm$ 1	14 $\pm$ 1	1150 $\pm$ 50
MS20	6.02 $\pm$ 1	12 $\pm$ 1	1480 $\pm$ 75
MS30	7.87 $\pm$ 1	4 $\pm$ 2	800 $\pm$ 75

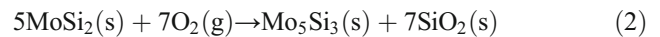
about 75 nm after milling. However, heat treatment leads to a partial increase in particle size. Furthermore, with increasing heat treatment time to 7 h at 1100 °C particle size increased to about 115 nm. The EDS analysis approved the existence of Mo, Si, and C elements.

Figure 5 shows the secondary electron (SE) and backscattered electron (BSE) microscopic images of the agglomerated MoSi<sub>2</sub>-SiC powders. Agglomeration process was employed for suitably of grain size and flow rate of composite powders as a feedstock for thermal spraying process. Figure 6 represents the EDS analyses of the specified points on Fig. 5d. A BSE study is also performed on Fig. 5d to determine the element distribution: the white, black, and gray areas corresponding to a high average atomic number were identified as Mo<sub>5</sub>Si<sub>3</sub>, SiC, and MoSi<sub>2</sub> phases, respectively. This behavior was further confirmed by the EDS analysis (Fig. 6). The EDS analyses are in accordance with the calculated weight fractions of MoSi<sub>2</sub> and Mo<sub>5</sub>Si<sub>3</sub> elements. The apparent density and flow rate of agglomerated powders were measured 0.96 g/cm<sup>3</sup> and 0.42 g/s, respectively. The changes in the average particle size of powders after different processes (Fig. 7) and results of apparent density and flow rate of agglomerated powders show that an agglomeration process is a beneficial method for suitably composite powders as a feedstock for thermal spraying process. Because of MA process, Fig. 7b shows the smallest particle size. The largest particle size was resulted after agglomeration process (Fig. 7d).

**Fig. 10** SEM image of the crack in the MS10 surface

## Characterization of the coatings

As shown in Fig. 8, the XRD patterns of the as-sprayed MoSi<sub>2</sub>-SiC coating with different amounts of SiC are composed of MoSi<sub>2</sub> tetragonal and hexagonal phases such as SiC, Mo<sub>5</sub>Si<sub>3</sub>, and SiO<sub>2</sub>. The MoSi<sub>2</sub> compound has two crystal structures; the tetragonal phase (C11b type) is a stable phase up to 1900 °C, above which it transforms to the hexagonal phase (C40 type) and melts congruently at 2030 °C [30]. Phase compositions of the coating are changed compared with the feedstock powder. A fraction of the tetragonal MoSi<sub>2</sub> was converted to hexagonal phase due to the high cooling rate of the deposited molten particles. The high-temperature hexagonal MoSi<sub>2</sub> phase was kept as the main phase in the coating. The existence of Mo<sub>5</sub>Si<sub>3</sub> phase is very likely due to oxidation of the MoSi<sub>2</sub> according to Eq. 2 [30].



The formation mechanism of MoSi<sub>2</sub> during the progression of the combustion method was suggested exothermic diffusional reactions between liquid Si and solid Mo when the compacts were preheated to a sample temperature of 1460 °C. In addition, Mo<sub>5</sub>Si<sub>3</sub> was the predominant phase formed prior to the melting of Si at low heating rates, the amount of MoSi<sub>2</sub> increased with increasing heating rate, and formation of Mo<sub>5</sub>Si<sub>3</sub> was negligible at a heating rate of 150 °C/min or above.

Surface morphologies of the as-sprayed MS20 coating are depicted in Fig. 9. Well-flattened lamellar along with some spherical features were observed on the surfaces of the coatings, which exhibit typical morphologies of plasma-sprayed coatings (Fig. 9a, b). As shown in Fig. 9c, the layer thickness is about 100  $\mu\text{m}$  and there is a good bond between coating and substrate.

According to the standard of adhesion strength of coatings (ASTM C0633 [24]), the thickness of the thermal spray coatings must be thick enough to prevent of bonding agent penetration into the coating pores and prevent errors in the test result. The minimum thickness of 380  $\mu\text{m}$  is recommended for strength samples [24, 31]. Therefore, the average thickness of coatings was considered 400  $\pm$  10  $\mu\text{m}$  after plasma spraying process for different tests.

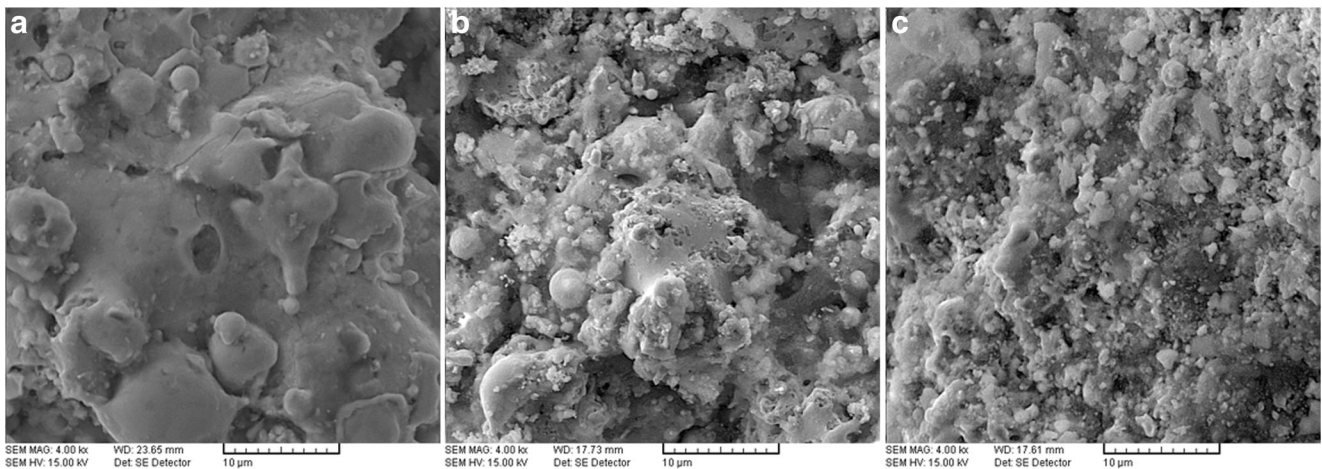


**Fig. 11** SEM images of the **a** MS10, **b** MS20, and **c** MS30 surfaces

Sandblasting process before spraying process is effective on the quality of the thermal spray coating [32]; the nickel substrates were sandblasted and then washed with acetone. The roughness of the substrates was measured  $0.17 \pm 1 \mu\text{m}$  and  $4.51 \pm 2 \mu\text{m}$  before and after sandblasting process,

respectively. Clearly, due to the blasting process, the roughness of nickel substrate was increased almost 26 times, which increases the adhesion of coatings.

Table 4 shows the results of roughness, microhardness, and adhesion strength measurements of the coatings. The high

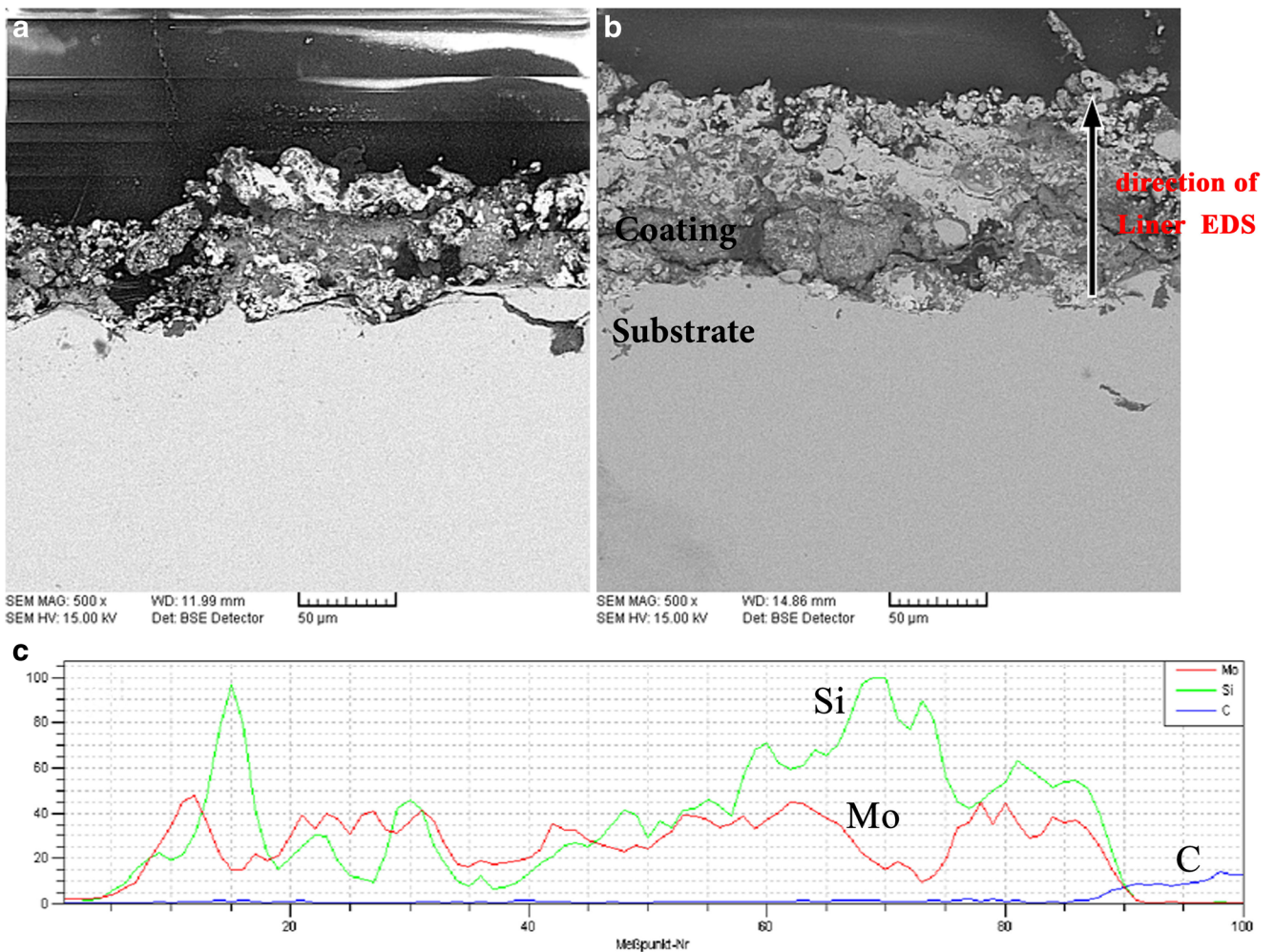


**Fig. 12** The polished cross section of the **a** MS10 and **b** MS20 coatings and **c** the liner EDS analysis of the MS20 coating

microhardness of the MS20 coating is attributed to the high hardness of SiC phase and the structure devoid of crack. As shown in Table 4, because of the high hardness of SiC phase, the microhardness of coatings was increased with an increase in SiC phase content to 20 vol%. The hardness of SiC phase is about 2800 Hv. Due to high porosity and weak bonding, the MS30 coating has shown the lowest microhardness.

According to Table 4, the adhesion strength of the different samples was decreased with SiC content increasing. The adhesion strength of APS ceramic coatings on metallic substrates is about 15 to 20 MPa [31]. In this investigation, because both MoSi<sub>2</sub> and SiC are ceramic and brittle; they provide acceptable adhesion strength results. Evaluation of the failure surfaces showed an intra-coating fracture. Hence, the adhesion between splats was lower than that between coating and substrate, and a good adhesion was observed between substrate and coating. Because of the weak connection between SiC and MoSi<sub>2</sub>, the interface of SiC–MoSi<sub>2</sub> can be a suitable place to crack and create separation during the adhesion strength test.

The SEM image of the MS10 surface (Fig. 10) shows some crack between splats caused due to the tensions by the rapid freezing of splats. In general, the inter-splat and intra-splat pores and cracks are the characteristics of thermal spray coating [33]. As shown in Fig. 11, the melting of the powder particles and thus broadening of the splats were reduced by increasing the reinforcement percentage. The polished cross section of the MS10 and MS20 coatings is shown in Fig. 12. The layered microstructure can be observed between splats that are common between thermal spray coatings. The porosity of the coatings was decreased with increasing the SiC contents. The EDS analysis of the MS20 coating indicates the existence of Si, Mo, and C elements in the specified direction. About MS30 sample, due to the excess SiC phase, the coating was separated from the substrate and destroyed.

## Conclusions

The MoSi<sub>2</sub>–SiC composite powders can be prepared by mechanically activated annealing synthesis through elemental powders. The results of this investigation show that the use of less expensive, although complex, Mo–Si–SiC powder mixture for the preparation of MoSi<sub>2</sub>–SiC by milling and heat treatment processes appears to be effective since homogeneous products with fine grain and particle sizes can be derived at reasonable cost and time.

In this study, MoSi<sub>2</sub>–SiC powders were deposited on nickel substrate using APS technique. The effect of the SiC content was studied on microstructural and mechanical properties of APS-ed coatings. Because of its microstructural and mechanical properties, the MS20 coating was chosen as the optimal sample. The greatest microhardness 1480 Hv was measured in

the MS20 sample, which corresponds to the high hardness of SiC particles. The surface roughness and adhesion strength of the optimal sample were measured 6.02 μm and 12 MPa, respectively.

**Publisher's note** Springer Nature remains neutral with regard to jurisdictional claims in published maps and institutional affiliations.

## References

- Xu, Y., Guan, Y., Zheng, Z., Tong, X.: Microstructure and tribological properties of plasma-sprayed nanostructured sulfide coating. *J. Mater. Sci. Technol.* **22**(5), 589–593 (2006)
- Chen, H., Zhou, X., Ding, C.: Investigation of the thermomechanical properties of a plasma-sprayed nanostructured zirconia coating. *J. Eur. Ceram. Soc.* **23**(9), 1449–1455 (2003)
- Wielage, B., Steinhäuser, S., Reisel, G., Morgenthal, I., Scholl, R.: Vacuum plasma spraying of prereacted MoSi<sub>2</sub> and SiC-reinforced MoSi<sub>2</sub> produced by a new kind of powder processing, 1st International Thermal Spray Conference: Thermal Spray Surface Engineering via Applied Research, ASM International, pp. 865–869 (2000)
- Tiwari, R., Herman, H., Sampath, S.: Vacuum plasma spraying of MoSi<sub>2</sub> and its composites. *Mater. Sci. Eng. A.* **155**(1–2), 95–100 (1992)
- Yao, Z., Stiglich, J., Sudarshan, T.: Molybdenum silicide based materials and their properties. *J. Mater. Eng. Perform.* **8**(3), 291–304 (1999)
- Petrovic, J.: Toughening strategies for MoSi<sub>2</sub>-based high temperature structural silicides. *Intermetallics.* **8**(9), 1175–1182 (2000)
- Hvizdos, P., Besterci, M., Balloková, B., Scholl, R., Böhm, A.: Creep behaviour of MoSi<sub>2</sub>–SiC and MoSi<sub>2</sub>–HfO<sub>2</sub>. *Mater. Lett.* **51**(6), 485–489 (2001)
- Radhakrishnan, R., Bhaduri, S., Henager, C.: The reactive processing of silicides. *JOM J. Miner. Met. Mater. Soc.* **49**(1), 41–45 (1997)
- Kang, P., Yin, Z.: Phase formation during annealing as-milled powders of molybdenum disilicide. *Mater. Lett.* **57**(28), 4412–4417 (2003)
- Krishnarao, R., Ramarao, V., Mahajan, Y.: In situ formation of MoSi<sub>2</sub>–SiC through reaction of SiO<sub>2</sub> or Si<sub>3</sub>N<sub>4</sub> with Mo and carbon. *J. Mater. Res.* **12**(12), 3322–3327 (1997)
- Sun, L., Pan, J.: Fabrication and characterization of TiC<sub>w</sub>/MoSi<sub>2</sub> and SiC<sub>w</sub>/MoSi<sub>2</sub> composites. *Mater. Lett.* **52**(3), 223–228 (2002)
- Morris, D.G., Leboeuf, M., Morris, M.: Hardness and toughness of MoSi<sub>2</sub> and MoSi<sub>2</sub>–SiC composite prepared by reactive sintering of powders. *Mater. Sci. Eng. A.* **251**(1), 262–268 (1998)
- Gedevanishvili, S., Munir, Z.: An investigation of the combustion synthesis of MoSi<sub>2</sub>β–SiC composites through electric-field activation. *Mater. Sci. Eng. A.* **242**(1), 1–6 (1998)
- Feng, P., Farid, A., Wang, X., Humail, I.S., Qu, X.: Mechanically activated reactive synthesis of refractory molybdenum and tungsten silicides. *Int. J. Refract. Met. Hard Mater.* **26**(3), 173–178 (2008)
- Suryanarayana, C.: Mechanical alloying and milling. *Prog. Mater. Sci.* **46**(1), 1–184 (2001)
- Gaffet, E., Abdellaoui, M., Malhouroux-Gaffet, N.: Formation of nanostructural materials induced by mechanical processings (overview). *Mater. Trans. JIM.* **36**(2), 198–209 (1995)
- Bakhshi, S.R.: Surface characteristics development of mechanically alloyed Mo–Si–B intermetallic compounds thermal spray coatings materials science and engineering, Isfahan University of Technology Isfahan (2009)

18. Erfanmanesh, M., Bakhshi, S.R.: Synthesis and characterization of nanocrystalline MoSi<sub>2</sub> by mechanical alloying and heat treating. *J. Clust. Sci.* **24**(1), 133–143 (2013)
19. ASTM B212–99, Standard test method for apparent density of free-flowing metal powders using the Hall Flowmeter funnel, ASTM International, West Conshohocken, PA (1999) [www.astm.org](http://www.astm.org)
20. ASTM B213–03, Standard test method for flow rate of metal powders, ASTM International, West Conshohocken, PA (2003) [www.astm.org](http://www.astm.org)
21. Erfanmanesh, M., Bakhshi, S.R., Khajelakzay, M., Salekbafighi, M.: The effect of argon shielding gas at plasma spray process on the structure and properties of MoSi<sub>2</sub> coating. *Ceram. Int.* **40**(3), 4529–4533 (2014)
22. Williamson, G.K., Hall, W.H.: X-ray line broadening from filed aluminium and wolfram. *Acta Metall.* **1**(1), 22–31 (1953)
23. Zakeri, M., Yazdani-Rad, R., Enayati, M.H., Rahimipoor, M.R.: Synthesis of MoSi<sub>2</sub>–Al<sub>2</sub>O<sub>3</sub> nanocomposite by mechanical alloying. *Mater. Sci. Eng. A.* **430**(1–2), 185–188 (2006)
24. ASTM C633–13, Standard test method for adhesion or cohesion strength of thermal spray coatings, ASTM International, West Conshohocken, PA (2013) [www.astm.org](http://www.astm.org)
25. Dorset, D.L.: X-ray diffraction: a practical approach. *Microsc. Microanal.* **4**(5), 513–515 (2005)
26. Safari, J., Akbari, G., Shahbazkhan, A., Chermahini, M.D.: Microstructural and mechanical properties of Al–Mg/Al<sub>2</sub>O<sub>3</sub> nanocomposite prepared by mechanical alloying. *J. Alloys Compd.* **509**(39), 9419–9424 (2011)
27. Mitra, R., Srivastava, A., Prasad, N.E., Kumari, S.: Microstructure and mechanical behaviour of reaction hot pressed multiphase Mo–Si–B and Mo–Si–B–Al intermetallic alloys. *Intermetallics.* **14**(12), 1461–1471 (2006)
28. Zhang, L., Sun, Z., Zhang, Y., Yang, W.: Thermodynamic and kinetic analysis of in situ synthesis of MoSi<sub>2</sub>–SiC composite. *Acta Metall. Sin.* **34**, 1205–1209 (1998)
29. Calka, A., Williams, J., Millet, P.: Synthesis of silicon nitride by mechanical alloying. *Scr. Metall. Mater.* **27**(12), 1853–1857 (1992)
30. Mitra, R.: Mechanical behaviour and oxidation resistance of structural silicides. *Int. Mater. Rev.* **51**(1), 13–64 (2006)
31. Pawlowski, L.: The science and engineering of thermal spray coatings, John Wiley & Sons (2008)
32. Taheri, M., Heydarzade, M., Ghadami, F.: Thermal spraying, Characteristics and applications, Rahpooyan Kherad, Tehran Iran (2009)
33. Heimann, R.B.: Plasma spray coating. Weinheim, New York (1996)